View metadata, citation and similar papers at core.ac.uk

brought to you by CORE

provided by NASA Technical Reports Server

7034

NASA/TM-1998- 207320

AIAA 98-0784

Direct Harmonic Linear Navier-Stokes Methods for Efficient Simulation of Wave Packets

C. L. Streett
NASA Langley Research Center
Hampton, VA

36th Aerospace Sciences Meeting & Exhibit

January 12–15, 1998 / Reno, NV

For permission to copy or republish, contact the American Institute of Aeronautics and Astronautics
1801 Alexander Bell Drive, Suite 500, Reston, Virginia 20191-4344

AIAA-98-0784

DIRECT HARMONIC LINEAR NAVIER-STOKES METHODS FOR EFFICIENT SIMULATION OF WAVE PACKETS[1]

C.L. Streett
NASA Langley Research Center
Hampton, VA, USA

Abstract

Wave packets produced by localized disturbances play an important role in transition in three-dimensional boundary layers, such as that on a swept wing. Starting with the receptivity process, we show the effects of wave-space energy distribution on the development of packets and other three-dimensional disturbance patterns. Nonlinearity in the receptivity process is specifically addressed, including demonstration of an effect which can enhance receptivity of traveling crossflow disturbances. An efficient spatial numerical simulation method is demonstrated for the computation of these flows, allowing most of the simulations presented to be carried out on a workstation.

Introduction

Over the past ten years, technology for the prediction of transition to turbulence in boundary layers has progressed well beyond the use of quasi-parallel linear stability theory, with the recognition that much of the disagreement between theory and experiment were the result of physical effects beyond the scope of such methods. Among these are: receptivity - the process by which external disturbance energy is internalized into disturbances which grow in the boundary layer; effects of nonparallelism and surface curvature; nonlinear transfer of energy between disturbance modes; and effects of local inhomogeneities on the growth of disturbances. While numerical simulation technology has progressed to the point that full spatial DNS of the transition process is at least feasible and has been carried out for a few select cases, examination of the above effects across a broad parameter range is impractical due to the expense of such simulations.

Many of these problems of interest may be cast in a linear or weakly-nonlinear framework, for which the modest spatial resolution requirements would render DNS a quite tractable tool for parametric studies. For the most part, only the steady-state results of such simulations are of interest; the start-up transients, which are always present in simulations carried out in the time-dependent formulation, contain little useful information regarding the long-time asymptotic state of transition of a given flow. For instance, if a time-dependent simulation of a single-frequency wave is carried out from an impulsive start of the harmonic "driver", then the transient will be observed as a leading-wave region which travels downstream; this region will consist of a broad spectrum of disturbances, initiated due to the step-function input. Each component wave will travel downstream at its characteristic group velocity, the slowest of which for the most part determines the length of the transient period. For many problems involving stationary or low-frequency disturbances, this period may be quite lengthy, and the simulation correspondingly expensive.

However, if the assumption is made that the disturbance field is comprised of only a few select frequencies, then efficient use can be made of many of the algorithmic elements of full spatial DNS, while enabling the use of fast direct linear solvers. The advantage of such a methodology is that solutions may be obtained rapidly on workstation-level machines, enabling a researcher to perform the desired parameter studies of complex transition physics. This paper is an overview of the use of one such implementation over the past five years; studies carried out have included the generation of validation data for engineering transition prediction methods including receptivity-prediction methods, the detailed design of hybrid laminar flow control suction surfaces, studies of linear and weakly-nonlinear wave packets, and computations of the effects of streamwise and spanwise inhomogeneities on the evolution of disturbances.

---

[1] This paper is declared a work of the U.S. Government and is not subject to copyright protection in the United States.

Algorithmic Aspects

What follows is a brief outline of the basic incompressible harmonic linear Navier-Stokes (HLNS) solver which was used in various forms to produce the results discussed below; a more complete description of the method will appear in a subsequent paper [1].

The first step in the formulation is expansion about a steady base flow:

$$\mathbf{u} = \mathbf{U}_b + \varepsilon\, \mathbf{u}'$$

where ε is assumed (for now) to be a small parameter. After substitution into the three dimensional incompressible Navier-Stokes equations, equations of like order are separated. The O(1) equations state that the base flow must satisfy the steady NS equations; however, we frequently use approximate solutions (such as solutions to the boundary-layer equations) for convenience, and for direct comparison with results from other methods. The $O(\varepsilon^2)$ equations contain the nonlinear terms, and are used to compute weakly-nonlinear corrections to the HLNS solutions. The $O(\varepsilon)$ equations, the linear disturbance equations, are of primary interest here. The use of a disturbance equation formulation is well-known to be required in computations of the initial stages of transition, as the accurate representation of the evolution of disturbances several orders of magnitude smaller than the base flow is essential.

The following assumptions are then utilized in the linear disturbance equations:

$$\partial \mathbf{u}'/\partial t = -i\omega\, \mathbf{u}' \qquad\qquad \partial \mathbf{u}'/\partial z = i\beta\, \mathbf{u}'$$

the first of which reflects the single-harmonic assumption, the second being the assumption of spanwise (z) homogeneity. The latter is directly useful for oblique disturbances in a two-dimensional base state, and for disturbances evolving within the infinite-swept wing framework. For more complex flows, a Fourier integral method is used to represent the spanwise dependencies, as will be discussed later.

The above process results in a complex two-dimensional equation set with two parameters: ω - related to the frequency of the disturbance, and β - the spanwise wavenumber. The streamwise (x) and normal (y) directions are discretized using relatively standard high-order methods: Chebyshev collocation is used in y, while fourth-order centered differences are used in x. These are natural choices given the solution scheme to be discussed below. Analytic mappings are used in both discretizations to improve resolution where required. Surface curvature is accounted for in the present method using the standard body-conforming thin-layer assumptions, which result in the simple addition of a few geometric factors to the Cartesian equation set; the Cartesian equations are smoothly recovered as the surface curvature becomes small.

The resulting complex algebraic system of equations are in the form of a block pentadiagonal system; the blocks are of size $4N_Y x 4N_Y$, and are full due to the spectral discretization in the y-direction. The key to the usability of this method is the efficient direct solution scheme developed for the discretized equation set; the system is solved using standard recursion, but the recursion coefficients computed during the forward-sweep phase are stored on disk. Asynchronous I/O, in which the actual disk operations are carried out simultaneously which the computation of the next set of coefficients, speeds the overall throughput. In an average computation with $N_X = 1200$ and $N_Y = 51$, a solution can be obtained in about 15 minutes on an SGI workstation; about 1.5 Gb of temporary disk storage is required.

Boundary conditions are a sensitive aspect of this formulation; it was found during the early development of this method that some boundary conditions which are commonly used for time-dependent simulations can result in spectacularly poor and meaningless results when applied in the harmonic framework. This is due to two reasons: First, the condition number of the system is large to begin with, since the terms on the diagonal are relatively small. A boundary condition set which would have the effect of merely limiting the maximum time step allowable in a time-dependent simulation could render the direct solution so contaminated by roundoff error as to be useless. Second, the harmonic solution is long-time asymptotic; outflow boundary conditions (in particular) which build spurious error slowly over time result in solutions dominated by the effect of reflections when applied to this framework. The buffer-domain method [2], in which the momentum equations are smoothly parabolized to convect disturbances through the outflow boundary, was found to be robust and reliable here.

Disturbance forcing is accomplished in many ways, depending on the particular physics being simulated. Regions or distributions of non-zero wall-normal velocity are used to simulate oscillating suction/blowing, for instance; formulations for receptivity simulations result in either non-zero surface tangential velocity or field-forcing, as discussed below.

Receptivity, the conversion of farfield disturbance energy into instability waves, results from the bilinear interaction between the unsteady signature of the farfield disturbance and a short-scale meanflow variation. In other words, a freestream disturbance of the proper frequency but long wavelength is scattered onto the short-wavelength instability spectrum by the local (steady) meanflow distortion of a surface inhomogeneity, such as a roughness element. See [3] for more details. The flowfield may be expanded as:

$$\mathbf{U}(x,y,t) \cong \mathbf{U}_b(X,y) + \varepsilon_w \mathbf{U}_w(x,y) + \varepsilon_{ac} \mathbf{U}_{ac}(x,y) e^{-i\omega t} + \varepsilon_w \varepsilon_{ac} \mathbf{U}_{w,ac}(x,y) e^{-i\omega t}$$

where the coordinate "X" in $\mathbf{U}_b(X,y)$ denotes slow variation in x. $\mathbf{U}_w$ may be computed for very small roughness heights using the HLNS solver with ω=0, and extrapolating the flow-tangency condition to y=0 to produce an inhomogeneous boundary condition on the tangential velocity:

$$U_w(x,0) = \partial U_b(X,0) / \partial y \bullet h(x)$$

where $h(x)$ is the normalized roughness shape. Alternatively, the full distorted steady field corresponding to $\mathbf{U}_b(X,y) + \varepsilon_w \mathbf{U}_w(x,y)$ may be computed directly using a Newton-iterated nonlinear-solver variant of the HLNS method, where the roughness geometry is represented exactly using a shearing transformation. As will be described later, the local effect on the evolution of the recepted instability wave of this distorted base flow is the dominant nonlinear effect when the roughness height ε_w is finite.

$\mathbf{U}_{ac}(x,y)$, the signature of the farfield disturbance, may be approximated in the case of acoustic receptivity by a Stokes wave; a more exact representation may be obtained through a solution of the linearized unsteady boundary-layer equations (LUBLE) [4]. Once $\mathbf{U}_{ac}$ and $\mathbf{U}_w$ are computed, their nonlinear interaction is used on the RHS of the HLNS solver for solution of the $\mathbf{U}_{w,ac}$ problem.

Since each (ω,β) component is computed independently in the linear formulation, wave packets may also be easily constructed. For instance, the disturbance produced by an isolated roughness which is compact in the z-direction has energy distributed in the β-plane; the Fourier integral of the bump shape provides the necessary wall-forcing as a function of β:

$$\hat{h}(\beta) = \sqrt{\frac{2}{\pi}} \int_0^\infty h(z) \cos(\beta z)\, dz$$

The Fourier integral is discretized using a Chebyshev collocation quadrature formula:

$$\hat{h}(\beta) \approx \sum_{j=0}^{N} h(z_j) \cos(\beta z_j)\, w_j$$

This discretization results in a set of $\{\beta_i\}$ at which the HLNS solutions are required. The packet is then constructed in the physical space via the inverse integral:

$$\mathbf{U}(x,y,z,t) = \sqrt{\frac{2}{\pi}} \int_0^\infty \hat{h}(\beta) \hat{\mathbf{U}}(x,y,\beta,t) \cos(\beta z)\, dz$$

$$\approx \sum_{i=0}^{N} \hat{h}(\beta) \hat{\mathbf{U}}(x,y,\beta_i,t) \cos(\beta z)\, w_i$$

Results

Crossflow Stability

As mentioned in the Introduction, the effects of streamline curvature and nonparallelism on the development of disturbances in three-dimensional boundary layers has been a significant concern in the development and application of transition prediction methods, especially for swept wings. Extensive use of the subject HLNS method has been made in the evaluation of these effects and in the calibration of advanced transition prediction tools.

To illustrate these effects, results are presented for crossflow disturbance growth in the boundary layer on the wing used in the ASU 45° swept-wing experiment [5], the pressure distribution for which is presented in Fig. 1. The modest favorable pressure gradient over the first 70% of the wing gives rise to consistent growth of crossflow disturbances over a relatively narrow band of spanwise wavenumbers, and napthaline surface flow visualization indicated the presence of strong stationary (ω = 0) crossflow disturbances. The effect of surface curvature on the evolution of one representative spanwise-wavenumber disturbance in terms of the local growth rate evaluated using the maximum streamwise disturbance velocity is shown in Fig. 2; for comparison, the result from a standard quasi-parallel linear stability theory (LST) calculation is also shown. Note that the effect of surface curvature is to significantly reduce the local growth rate in this region near the leading edge; farther downstream, the two HLNS results merge as the curvature decreases. The large increase in growth rate shown by the HLNS results near the leading edge stem from the strong nonparallel effect, as the boundary layer grows rapidly in the first 5%-chord arclength from the attachment line. The fact that the LST and HLNS results appear to agree after about x/c = .07 is completely fortuitous; results for other flowfields show significant disagreement between the very approximate LST and the virtually exact (for linear disturbance evolution) HLNS method. An additional result for this flowfield is shown in Fig. 3; in this figure, a comparison between HLNS, PSE and LST results is made. Although the PSE results show some effect due to boundary-layer nonparallelism, this effect is still underestimated. Also shown in the figure is the effect of changing the streamwise placement of the suction/blowing strip which was used in the HLNS calculations to initiate the crossflow disturbance.

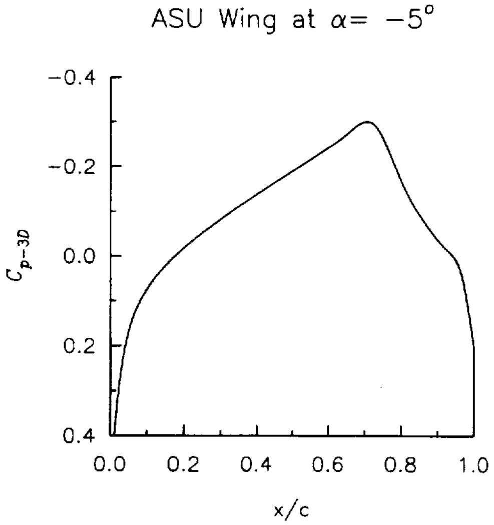

Figure 1 Pressure distribution on ASU swept wing

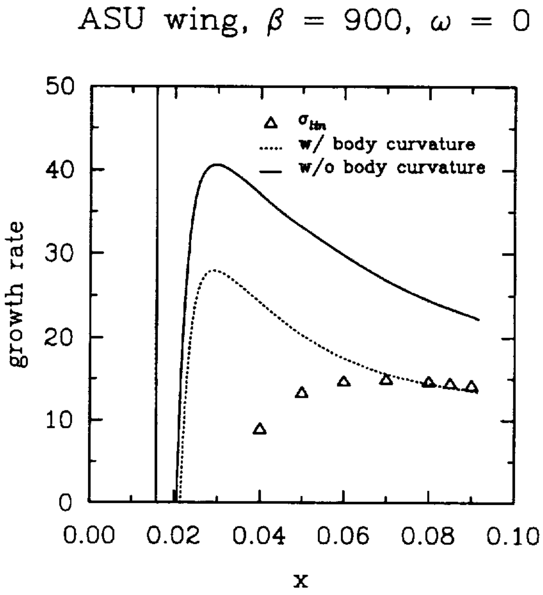

Figure 2 Stationary crossflow growth rate

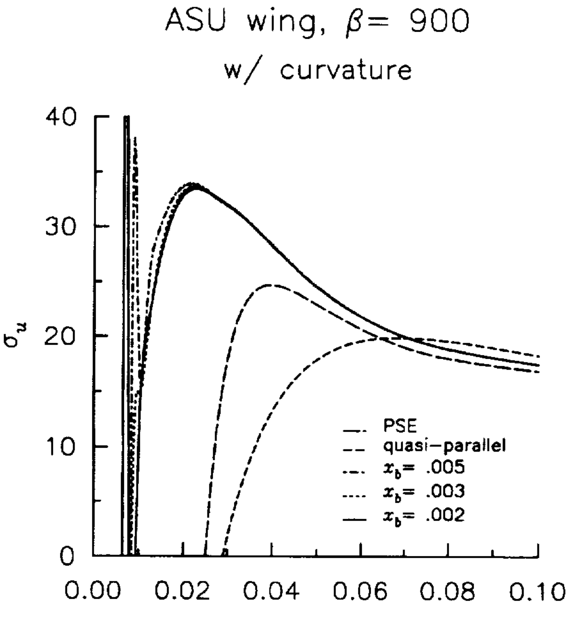

Figure 3 Stationary crossflow growth rate, comparison of LST, PSE, and HLNS

Crossflow Receptivity - Packets

Significant use of the HLNS method to predict the receptivity and evolution of crossflow disturbances in the presence of localized suction was made during the design and execution of a NASA / Boeing hybrid laminar flow control (HLFC) swept-wing experiment [6]; results from this test are proprietary, but overall indicated that standard LST transition prediction methods are quite unsatisfactory for use in swept-wing flows.

The computation of the development and evolution of a packet of crossflow disturbances behind a roughness element near the leading edge of a swept wing will serve as an example of the use of the spanwise Fourier-integral method described above. A surface bump, circular in plan and Gaussian in cross-section, was represented using linear boundary conditions near the attachment line in a swept-wing boundary layer. Fig. 4 shows a plan view of isosurfaces of the streamwise component of disturbance velocity, red denoting positive and blue negative, with the lateral boundaries of the displayed computational region being parallel to the freestream direction and the inflow boundary (left) parallel to the leading edge of the wing. A particular pressure distribution was chosen for the infinite-swept mean flow which results in a rather wide-band growth of crossflow disturbances, and the small-scale roughness element which induces the disturbance packet in the computation creates initial energy in a range of scales which includes this growth band. The small variation of wave angle and growth direction across this band of growing crossflow disturbances is visible in the downstream evolution of the packet; disturbances with small spanwise wavelength appear on the downstream side of the packet, whereas those of longer wavelength propagate on the windward side. This effect is more apparent in Fig. 5, in which disturbance streamwise velocity from cuts at various chordwise locations is shown.

Similarly, the initiation of stationary crossflow disturbances by perforated suction surfaces may be computed. In Fig 6 are shown isosurfaces of positive and negative disturbance velocity for flow of a swept-wing boundary layer over a spanwise-periodic array of suction holes; the 7 rows of holes in the simulation are evident in the figure. For this case, the spacings and angles of the rows of holes were chosen to produce near alignment of the holes along constant disturbance-phase lines, resulting in constructive interference of the waves from one row to the next. Simulations of this type have been used to study the performance sensitivity of perforate patterns for use in HLFC applications.

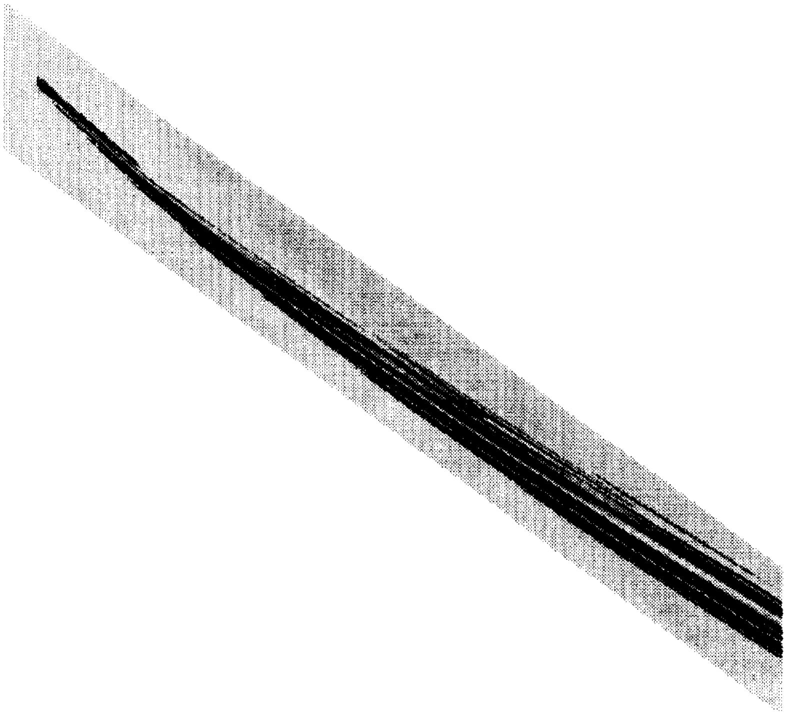

Figure 4 Isosurfaces of disturbance velocity behind roughness element on swept wing.

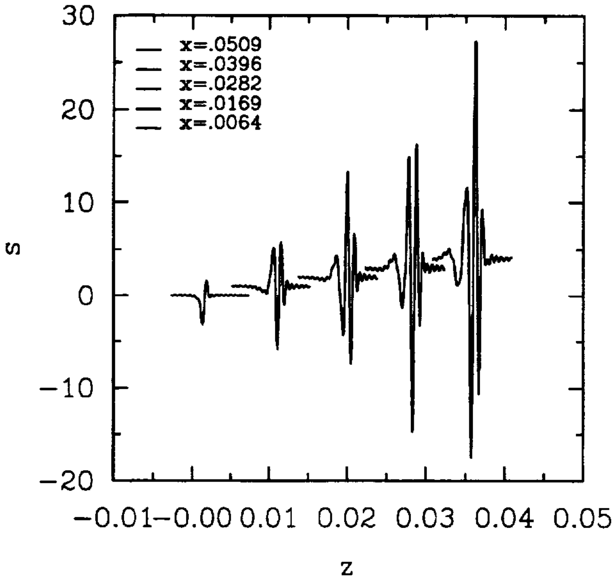

Figure 5 Crossflow packet disturbance velocity at various chordwise locations.

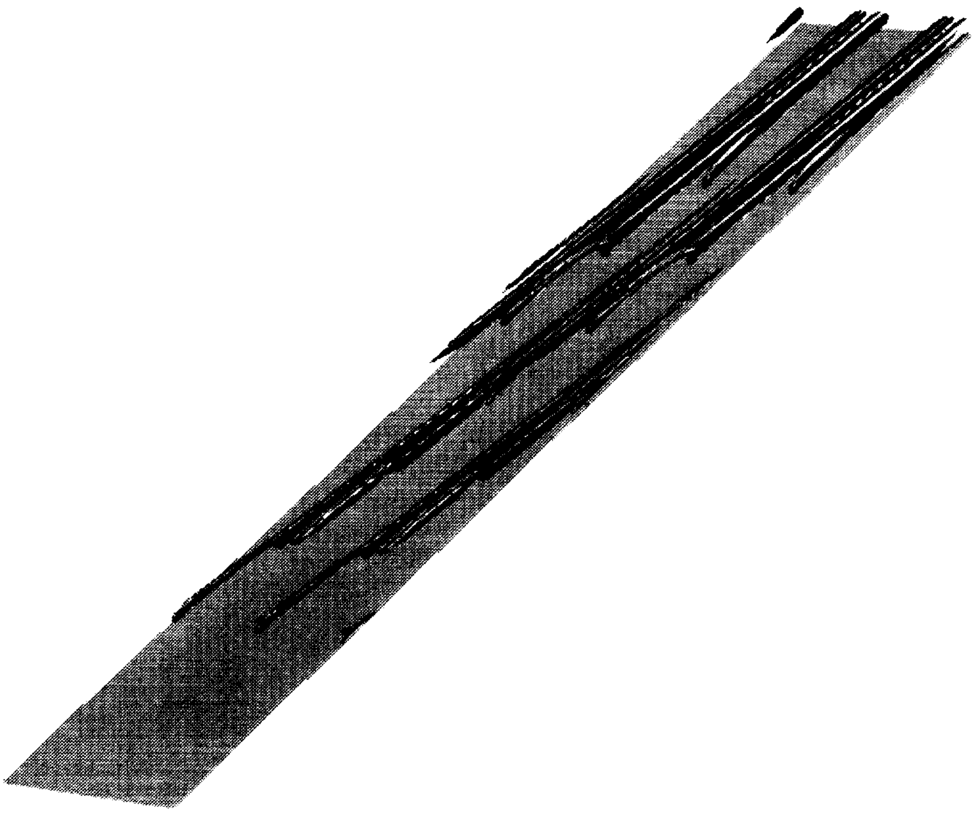

Figure 6 Disturbance velocity isosurfaces, perforated suction surface.

Effect of Spanwise Meanflow Distortion

When a stationary crossflow disturbance of a particular spanwise wavenumber β_w evolves in a meanflow field that contains a small-amplitude slow spanwise variation, the disturbance is distorted. This distortion may be approximated, if the spectrum of the spanwise variation of the meanflow is confined to small wavenumbers, by the bilinear scattering of the β_w into sidebands. For instance, if the meanflow variation possesses only a single spanwise component β_0, then this bilinear interaction forces sideband disturbances of spanwise wavenumber $\beta_w \pm \beta_0$. If β_0 is sufficiently small, these sideband disturbances will grow on their own, since their spanwise wavenumbers will lie in the same unstable range as the original disturbance. Thus, only a short streamwise region of meanflow variation is necessary to produce a disturbance field with rich spanwise content.

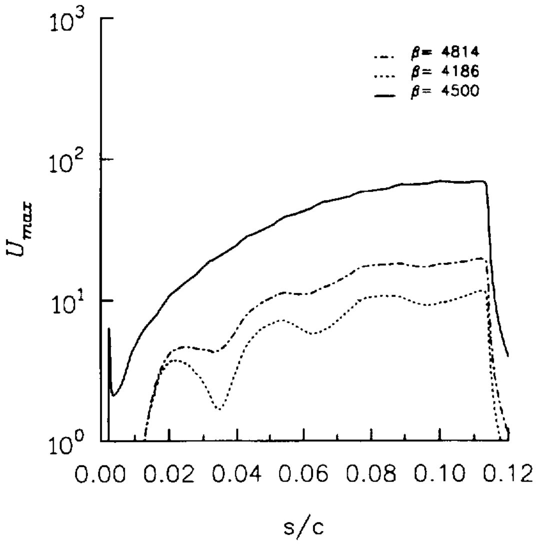

Figure 7 Disturbance amplitude, effect of spanwise meanflow distortion on stationary crossflow disturbance

The simple bilinear interaction is demonstrated by the example of a single crossflow disturbance, initiated by a roughness strip, evolving into an unstable mean boundary layer on which a 1%-amplitude distortion with small spanwise wavenumber is imposed. In Fig. 7 is plotted the growth of the streamwise component of disturbance velocity; the initiation of the original wave (β_w=4500) is apparent near the leading edge. The spanwise distortion of the meanflow occurs over the region .01 ≤ s/c; note that the scattered sideband disturbances grow rapidly to nearly comparable amplitude of the original disturbance. However, since the continued forcing of these waves is at a slightly different streamwise wavenumber than the disturbances which grow at the sideband spanwise wavenumbers (β = 4186 & 4814), constructive and destructive interference occurs in the evolution of these waves. The reconstructed disturbance flowfield shows the expected spanwise variation in amplitude, as seen in Fig. 8.

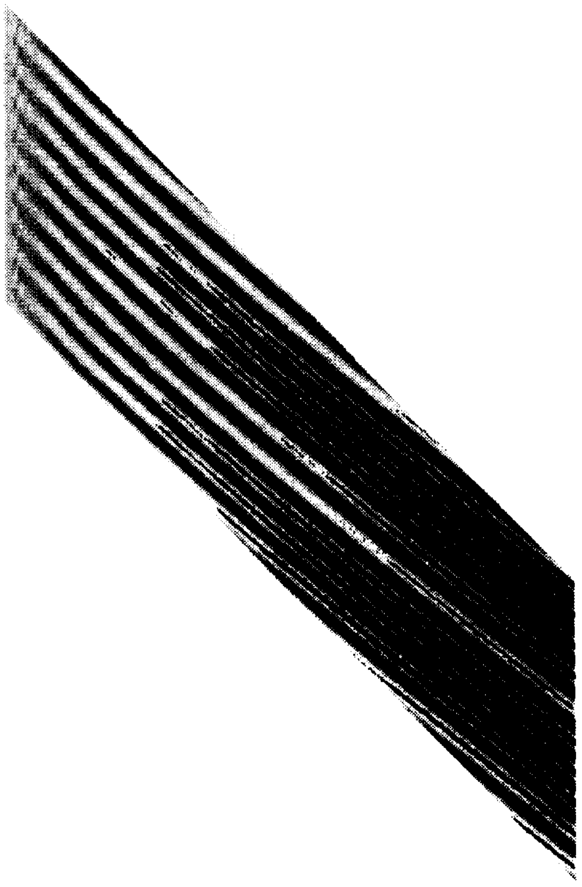

Figure 8 Contours of disturbance velocity, corresponding to Fig. 7

Nonlinear Receptivity

The HLNS method has also been used extensively in the calibration of receptivity-prediction methods and theories, to be used in engineering amplitude-prediction tools for transition prediction. As described above, both linear and weakly nonlinear acoustic receptivity predictions are possible using HLNS methods. Two examples of receptivity of two-dimensional TS waves are shown here, the first resulting from a roughness strip, the second from a suction slot. The first case, shown in Fig. 9 in terms of receptivity coefficient against roughness height, indicates that the finite-Reynolds number local method of Choudhari, *et al* [7], is in complete agreement with the purely linear simulation result; however, significant deviation is seen between these results and the experimental results of Saric, *et al* [8]. The weakly nonlinear results, in which the effect of the roughness distortion on the local stability of the disturbance is taken account, shows much better agreement. Similarly, the local and HLNS results agree well for the suction-slot case shown in Fig. 10; however, the local-stability modification effect is even stronger for this case, and the weakly-nonlinear results deviate from the linear results significantly even for small suction rates

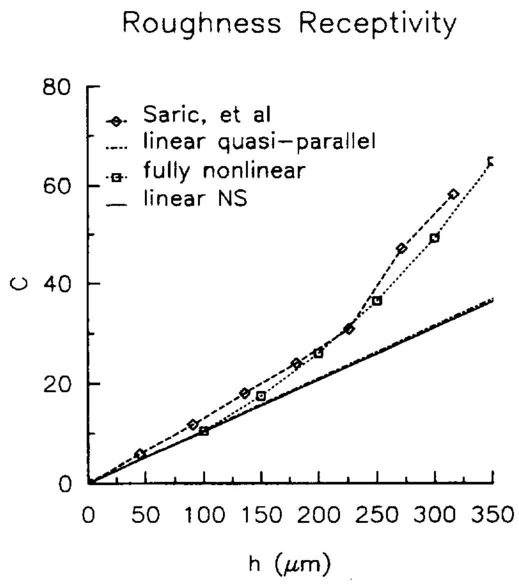

Figure 9 Roughness receptivity coefficient

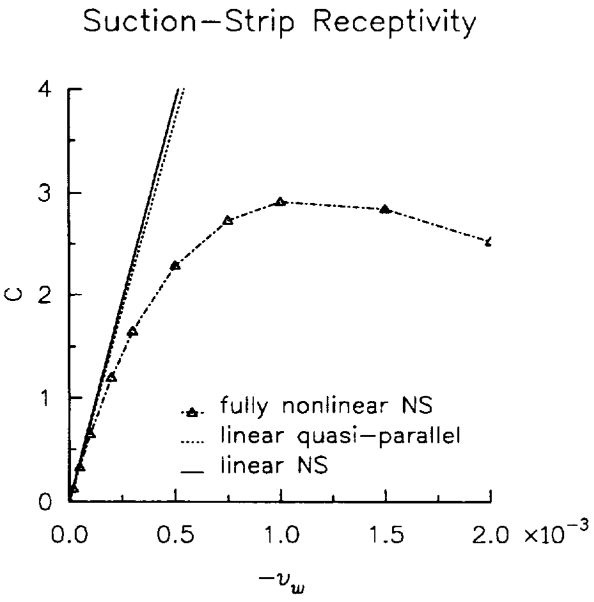

Figure 10 Suction receptivity coefficient

Distributed Receptivity

Since the surface roughness distribution may be specified arbitrarily in the HLNS predictions, distributed roughness receptivity effects are easily simulated. Shown in Fig. 11 is the disturbance amplitude $\max_y\{U_{w,ac}(x,y)\}$ (without roughness height and acoustic amplitude parameters ε_w and ε_{ac}), corresponding to the experiment of Wiegel and Wlezien [9] in which a series of tape strips were placed at spacings corresponding to the wavelength of the TS wave excited at the acoustic-driver frequency in a flat-plate boundary layer. The receptivity saturation observed in that experiment, and predicted by an extension of the local receptivity theory [10], is apparent.

When the relative phases of waves induced by individual roughness elements in a distributed-receptivity situation do not precisely correspond, the receptivity is "detuned" and significantly weaker. Of course, for true distributed roughness on an aircraft surface, detuning would always be present and must be predicted, at least in the mean. An example of this detuning is shown in Fig. 12, in which the TS disturbance amplitude for acoustic receptivity at a particular frequency over a wavy wall is shown, first for the case in which the acoustic frequency corresponds to the wavelength of the wall, and second for the case in which the wavelength of the wall is 10% shorter. Evident is the destructive interference between the waves produced in the leading part of the wavy-wall region (denoted by the filled triangles) with the waves produced later in the region. Work in this area of distributed-roughness receptivity, especially for the case of stationary crossflow receptivity, is continuing using statistical models of roughness measured directly from surfaces of various levels of finish.

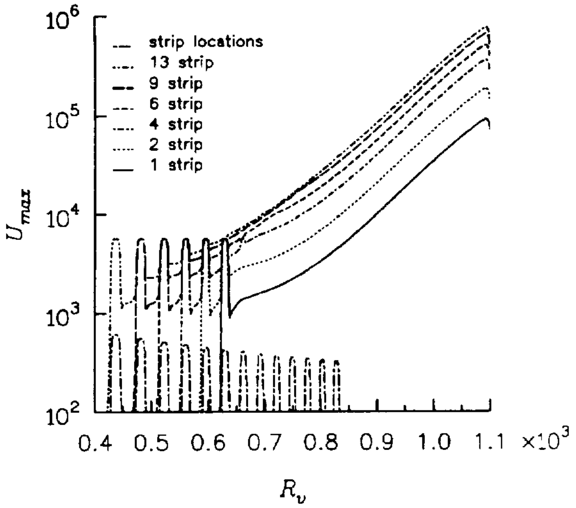

Figure 11 Disturbance amplitude, distributed roughness receptivity

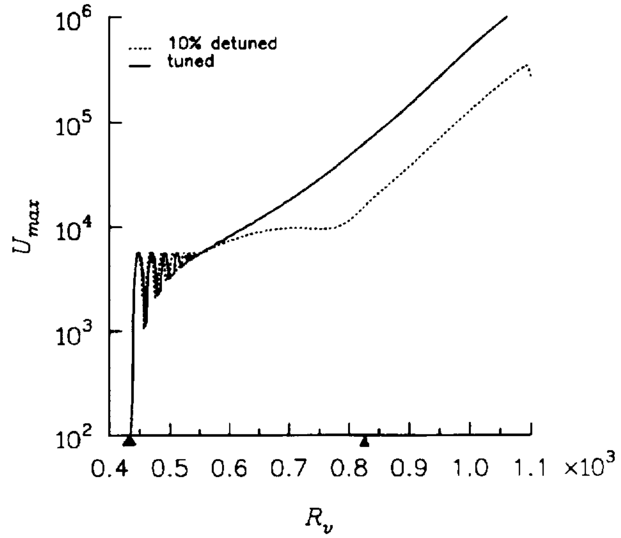

Figure 12 Disturbance amplitude, tuned and detuned wavy-wall receptivity

Nonlinear Crossflow Receptivity

In the case of traveling (i.e. non-zero frequency) crossflow disturbances, it was noted that the full distorted steady field corresponding to $\mathbf{U}_b(X,y) + \varepsilon_w \mathbf{U}_w(x,y)$ in the above formulation should also include the finite-amplitude stationary crossflow disturbance recepted by the roughness, as well as the nonlinear local distortion produced directly by the roughness. Since the streamwise wavenumber of the stationary disturbance is slightly different than that of the traveling disturbance, the interaction of the stationary disturbance with the Stokes' wave produces an additional receptivity mechanism that is detuned. This detuning results in an oscillatory amplitude increment over what would result from the interaction of the Stokes' wave with the local roughness flowfield distortion. An example of this additional receptivity is shown in Fig. 13, for the case of a roughness strip with a particular spanwise wavelength, positioned near the leading edge of the ASU swept wing. Note that there are regions in which this additional receptivity mechanism adds an order of magnitude to the amplitude of the traveling crossflow disturbance, and that this increment is not a function of either ε_w or ε_{ac}.

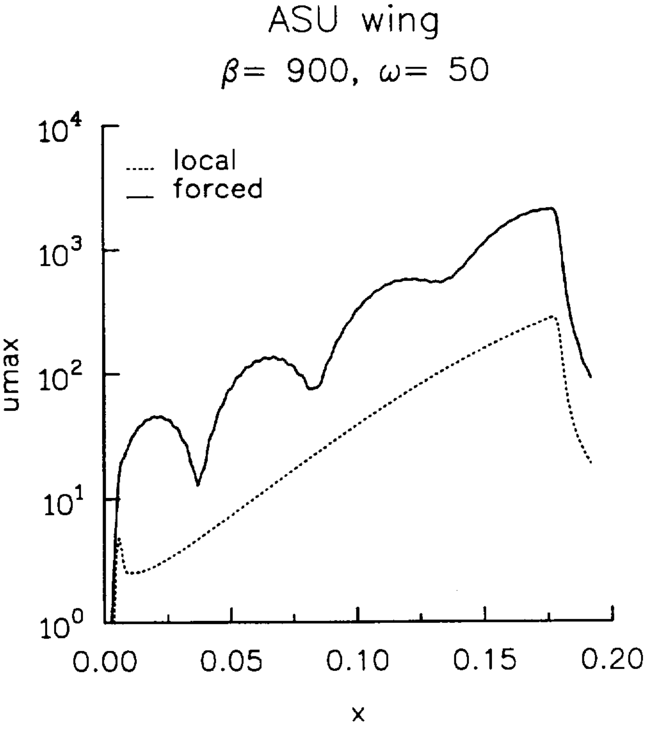

Figure 13 Disturbance amplitude, nonlinear traveling crossflow receptivity

Harmonic Point Source

In 1995, Watmuff [11] published results from very high resolution hot-wire measurements of the wave packet produced by oscillatory suction and blowing through a small hole in the surface under a flat-plate boundary layer. Ostensibly for studying the effect of discrete suction used for laminar flow control, the data provides an excellent test for approximate simulation methods. Initial comparisons with wave packets generated by summation of modes from linear stability theory, and with packets computed using the linear parabolized stability equations (PSE), showed that even for the small amplitude used in the experiment, some nonlinearity was present. This may be seen by comparing the isosurfaces of streamwise disturbance velocity from the experiment (Fig. 14) with those from the summation of 17 (symmetric) spanwise modes computed using the HLNS method (Fig. 15). Although the general wave pattern is captured by the linear computation, the experiment shows some detail on the centerline which is missing in the linear results; additionally, the experimental wave fronts are somewhat flatter than seen in the linear computation.

Based on the conjecture that the disagreement was due to stabilizing meanflow distortion near the centerline of the packet, a nonlinear harmonic Navier-Stokes computation was carried out, in which only the primary, zero-frequency, and first harmonic temporal modes were included. The computation was done in a brute-force iterative manner, with the values of the nonlinear terms for each spanwise and temporal harmonic mode calculated from the previous global iteration and carried as forcing functions. These forcing functions were computed by exact decomposition for the temporal terms, and by reconstructing the total flowfield in successive streamwise planes, computing the nonlinear terms, and performing a spanwise FFT; the spanwise grid used for reconstruction used twice the number of spanwise modes, to dealias the computation. The results of this ongoing computation are shown in Fig. 16; the results near the centerline agree far better with the experiment, demonstrating the stabilization by the zero-frequency component; the computation does, however, suffer from lack of spanwise resolution.

Conclusions

A number of example applications of the HLNS method have been presented. It should be recalled that all of the results shown were computed on workstation-level hardware, and that broad parameter studies for many of the physical aspects of transition on swept wings discussed here have been carried out using a suite of codes developed around this method. Additionally, weakly nonlinear effects on disturbance growth, secondary instability, and disturbance scattering by meanflow distortions have also been computed using this method; these will be described in subsequent papers.

References

1. Streett, C.L., "Direct Harmonic Navier-Stokes Methods for Efficient Simulation of Weakly-Nonlinear Wave Packets," AIAA Paper 98-0784, 1998.
2. Streett, C.L., and Macaraeg, M.G., "Spectral Multidomain for Large-Scale Fluid Dynamic Simulations," *Int. J. Appl. Numer. Math.*, **6**, pp. 123-140, 1989.
3. Goldstein, M.E., "Scattering of Acoustic Waves into Tollmien-Schlichting Waves by Small Streamwise Variations in Surface Geometry," *J. Fluid Mech..*, **154**, pp. 509-529, 1985.
4. Ackerberg, A. and Phillips, G., "The Unsteady Laminar Boundary Layer on a Semi-Infinite Flat Plate due to Small Fluctuations in the Magnitude of the Free-Stream Velocity," *J. Fluid Mech.*, **51**, pp. 137-157, 1972.
5. Dagenhart, J.R., Saric, W.S., Mousseux, M.C., and Stack, J.P., "Crossflow-Vortex Instability and Transition on a 45-Degree Swept Wing," AIAA Paper 89-1892, 1989.
6. Phillips, E.H., "NASA Sends Test Data Via Web," *Aviation Week & Space Technology*, April 15, 1996.
7. Choudhari, M., and Streett, C.L., "A Finite Reynolds Number Approach for the Prediction of Boundary Layer Receptivity in Localized Regions," NASA TM 102781, Jan. 1991.
8. Saric, W.S., Hoos, J.A., and Kohama, Y., "Boundary Layer Receptivity: Part I. Freestream Sound and 2-D Roughness Strips," College of Engineering and Applied Sciences Report CEAS-CR-90191, Arizona State University, 1990.
9. Wiegel, M., and Wlezien, R.W., "Acoustic Receptivity of Laminar Boundary Layers over Wavy Walls," AIAA Paper 93-3280, 1993.
10. Choudhari, M., "Boundary-Layer Receptivity due to Distributed Surface Imperfections of a Deterministic or Random Nature," *Theoret. Comput. Fluid Dyn.*, **4**, pp. 101-118, 1993.
11. Watmuff, J., "Boundary Layer Transition Studies," MCAT Report NCC2-698-95-12, February, 1995.

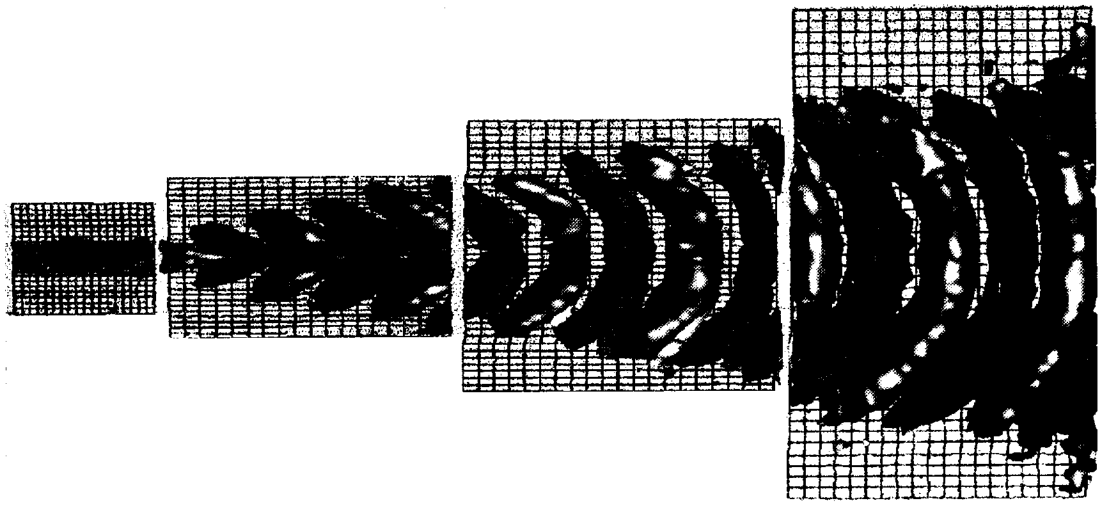

Figure 14 Isosurfaces of disturbance velocity, Watmuff HPS experiment

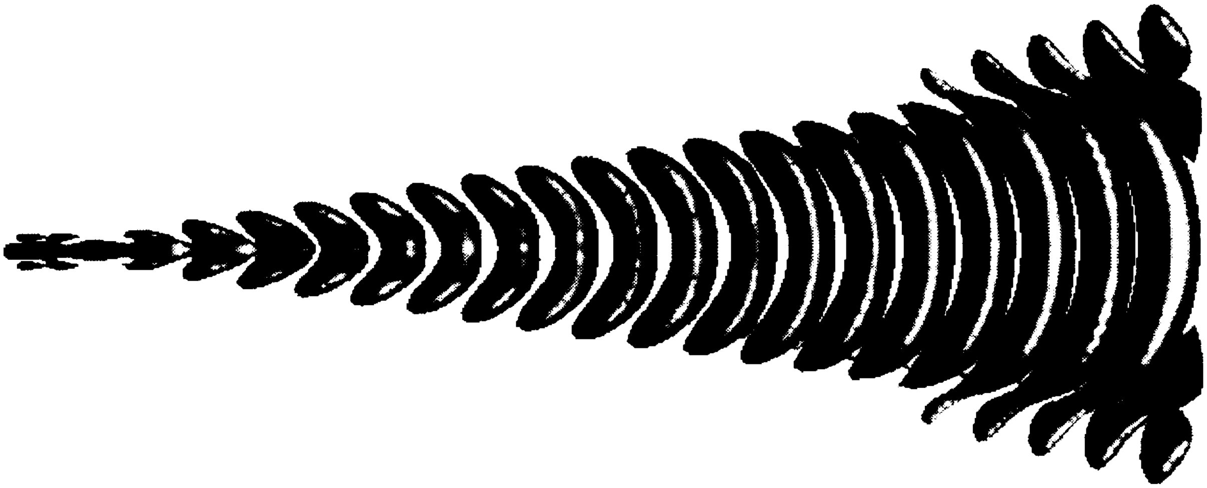

Figure 15 Isosurfaces of disturbance velocity, linear HLNS computation

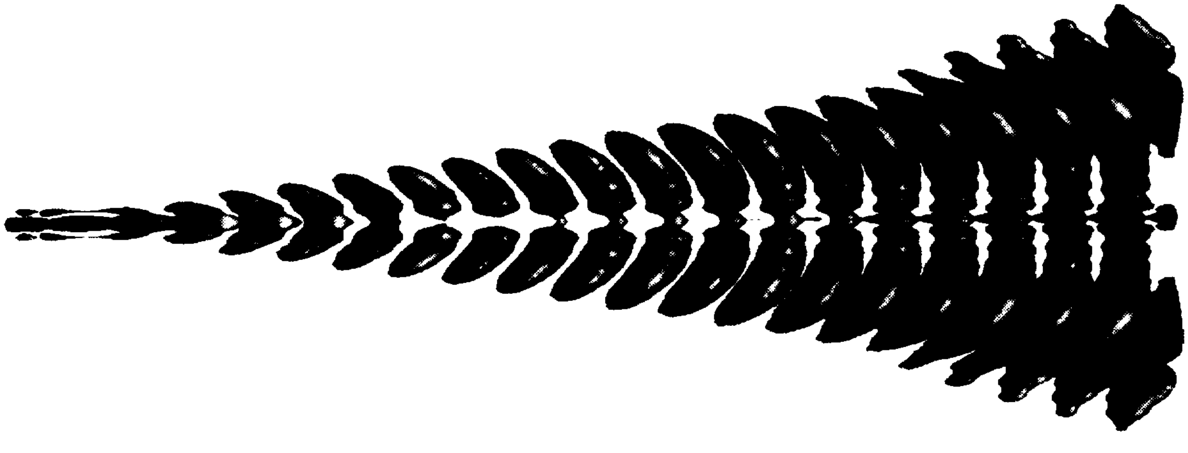

Figure 16 Isosurfaces of disturbance velocity, nonlinear harmonic N-S computation